Inorganic Chemistry
Article

Inorg. Chem. **2010**, *49*, 11499–11504 **11499**
DOI: 10.1021/ic101608b

Highly Uniform and Monodisperse $Gd_2O_2S:Ln^{3+}$ (Ln = Eu, Tb) Submicrospheres: Solvothermal Synthesis and Luminescence Properties

Yanhua Song, Hongpeng You,* Yeju Huang, Mei Yang, Yuhua Zheng, Lihui Zhang, and Ning Guo

State Key Laboratory of Rare Earth Resource Utilization, Changchun Institute of Applied Chemistry, Chinese Academy of Sciences, 130022, P.R. China and Graduate University of the Chinese Academy of Sciences, Beijing 100049, P.R. China

Received August 9, 2010

$Gd_2O_2S:Ln^{3+}$ (Ln = Eu, Tb) submicrospheres were successfully prepared through a facile and mild solvothermal method followed by a subsequent heat treatment. X-ray diffraction (XRD) results demonstrate that all the diffraction peaks of the samples can be well indexed to the pure hexagonal phase of Gd_2O_2S. The energy dispersive spectroscopy (EDS), element analysis, and FT-IR results show that the precursors are composed of the Gd, Eu, O, S, C, H, and N elements. The scanning electron microscopy (SEM) and transmission electron microscopy (TEM) results show that these spheres are actually composed of randomly aggregated nanoparticles. The formation mechanism for the $Gd_2O_2S:Ln^{3+}$(Ln = Eu, Tb) spheres has been proposed on an isotropic growth mechanism. Under ultraviolet excitation, $Gd_2O_2S:Ln^{3+}$(Ln = Eu, Tb) spheres show red and green emission corresponding to the $^5D_0 \rightarrow {}^7F_2$ transition of the Eu^{3+} ions and the $^5D_4 \rightarrow {}^7F_5$ transition of the Tb^{3+} ions. Furthermore, this synthetic route may have potential applications for fabricating other lanthanide oxysulfides.

1. Introduction

Lanthanide compounds, such as hydroxides,[1] oxides,[2] phosphates,[3] fluorides,[4] oxysulfides,[5] and vanadates,[6] have been extensively studied because of their potential applications as high-performance magnets, luminescent devices, catalysts, and other functional materials based on the electronic, magnetic, optical, and chemical characteristics arising from their f electrons.[7] Among them, the lanthanide (La−Lu) oxysulfides with high chemical stability and high thermal stability are known as wide-gap (4.6−4.8 eV) materials.[8] They are also efficient phosphors with a broad excitation band. Therefore, Eu^{3+} activated lanthanide oxysulfides become a very important family of inorganic materials that have potential applications in various fields, such as color television picture tubes, radio-graphic imaging, field emission displays, and long-lasting phosphorescence.[9]

Conventionally, Ln_2O_2S (Ln = La, Pr, Nd, Eu, Gd, Tb) could be synthesized by the reaction of rare-earth oxide with S gas or CS_2 in the temperature range 597−1027 °C. In addition, the Eu-doped Ln_2O_2S phosphor materials were prepared by rare-earth oxides with elemental sulfur and flux (Na_2CO_3) at 1100 °C in a reduced atmosphere for 2 h or by direct thermal decomposition of the respective oxalate compounds under Ar and S vapor.[10] However, the subsequent grinding generally degrades luminescent efficiencies because of the introduction of surface defects that act as non-radiative recombination centers, and the morphology of the powder is often irregular.[11] More recently, many efforts have been directed toward the design and synthesis of lanthanide chalcogenides at the nanoscale stimulated by their interesting properties which differ from those of the bulk materials. Nano to micro scale $Ln_2O_2S:Eu^{3+}$ (Ln = Y, La, and Gd) with different morphologies have been synthesized by

*To whom correspondence should be addressed. E-mail: hpyou@ciac.jl.cn.

(1) Xu, A. W.; Fang, Y. P.; You, L. P.; Liu, H. Q. *J. Am. Chem. Soc.* **2003**, *125*, 1494.
(2) (a) Si, R.; Zhang, Y. W.; You, L. P.; Yan, C. H. *Angew. Chem, Int. Ed.* **2005**, *44*, 3256. (b) Cao, Y. C. *J. Am. Chem. Soc.* **2004**, *126*, 7456. (c) Yu, T.; Joo, J.; Park, Y. I.; Hyeon, T. *Angew. Chem., Int. Ed.* **2005**, *44*, 7411.
(3) Heer, S.; Lehmann, O.; Haase, M.; Güdel, H. U. *Angew. Chem., Int. Ed.* **2003**, *42*, 3179.
(4) (a) Zhang, Y. W.; Sun, X.; Si, R.; You, L. P.; Yan, C. H. *J. Am. Chem. Soc.* **2005**, *127*, 3260. (b) Burns, J. H. *Inorg. Chem.* **1965**, *6*, 881. (c) Boyer, J. C.; Vetrone, F.; Cuccia, L. A.; Capobianco, J. A. *J. Am. Chem. Soc.* **2006**, *128*, 7444. (d) Yi, G. S.; Chow, G. M. *Chem. Mater.* **2007**, *19*, 341. (e) Sudarsan, V.; Sivakumar, S.; van Veggel, F. C. J. M.; Raudsepp, M. *Chem. Mater.* **2005**, *17*, 4736.
(5) Jüstel, T.; Nikol, H.; Ronda, C. *Angew. Chem., Int. Ed.* **1998**, *37*, 3084.
(6) (a) Huignard, A.; Buissette, V.; Laurent, G.; Gacoin, T.; Boilot, J. P. *Chem. Mater.* **2002**, *14*, 2264. (b) Jia, C. J.; Sun, L. D.; Luo, F.; Jiang, X. C.; Wei, L. H.; Yan, C. H. *Appl. Phys. Lett.* **2004**, *84*, 5305.
(7) Jia, G.; You, H.; Liu, K.; Zheng, Y.; Guo, N.; Jia, J.; Zhang, H. *Chem.—Eur. J.* **2010**, *16*, 2930.
(8) Mikami, M.; Oshiyama, A. *J. Lumin.* **2000**, *87−89*, 1206.
(9) Dai, Q.; Song, H.; Wang, M.; Bai, X.; Dong, B.; Qin, R.; Qu, X.; Zhang, H. *J. Phys. Chem. C* **2008**, *112*, 19399.
(10) Yu, S. H.; Han, Z. H.; Yang, J.; Zhao, H. Q.; Yang, R. Y.; Xie, Y.; Qian, Y. T.; Zhang, Y. H. *Chem. Mater.* **1999**, *11*, 192.
(11) Abrams, B. L.; Holloway, P. H. *Chem. Rev.* **2004**, *104*, 5783.

Published on Web 11/24/2010

sol−gel method,[12−15] combustion,[9] conversion via the boron−sulfur method,[16] solvothermal pressure-relief method,[10] thermal decomposition of the precursor of $Ln(phen)(ddtc)_3$ (phen = 1, 10-phenanthroline; ddtc = diethyldithiocarbamate), and conversion of $Gd(OH)_3$ method.[17] But to the best of our knowledge, spherical lanthanide oxysulfides have been rarely reported to date because of the great difficulty in finding an effective synthetic route.[17] However, it is well-known that uniform, spherical phosphor powders favored in the screening process are desirable for high-quality display devices.[18] In recent years, the hydrothermal/solvothermal process has been widely used to prepare nano- or micrometer sized particles with uniform size and shape. Some monodisperse nano/microspheres were successfully synthesized through the surfactant-assisted hydrothermal/solvothermal process.[19]

In this paper, we report the preparation of spherical $Gd_2O_2S:Ln^{3+}$ (Ln = Eu, Tb) materials through a facile solvothermal process by subsequent heat treatment process. A phenomenological growth mechanism for the submicrospheres is proposed. Finally, we investigate the photoluminescence properties of $Gd_2O_2S:Eu^{3+}$ and $Gd_2O_2S:Tb^{3+}$. This synthetic route is also suitable for fabricating other lanthanide oxysulfide.

2. Experimental Section

2.1. Preparation. The rare-earth oxides RE_2O_3 (RE = Gd, Eu) (99.99%) and Tb_4O_7 (99.99%) were purchased from Shanghai Yuelong Non-Ferrous Metals Limited. The other chemicals were purchased from Beijing Chemical Co., and all chemicals are analytical grade reagents and used directly without further purification. Rare-earth nitrate stock solutions were prepared by dissolving the corresponding metal oxide in nitric acid at elevated temperatures. In a typical procedure, 3.9 mL of $Gd(NO_3)_3$ (0.5 M) and 1 mL of $Eu(NO_3)_3$ (0.05 M) were added into 25 mL of ethylene glycol (EG), then 2.0 g of poly(vinyl pyrrolidone) (PVP K30, M = 40000) was added into the above solution. After vigorous stirring for 10 min, the PVP was dissolved thoroughly. Then 10 mL of ethanol solution containing 0.11 g of thiourea was added dropwise into the above solution. The as-obtained solution was stirred for another 30 min. Then the transparent feedstock was transferred to a 50 mL Teflon-lined stainless autoclave and heated at 200 °C for 24 h. After naturally cooling to room-temperature, the precursors were separated by filtration, washed with ethanol and deionized water five times, and dried in atmosphere at 60 °C overnight. The final products were obtained through a heat treatment at desired temperatures (600−800 °C) for 2 h under an inert N_2/S atmosphere.

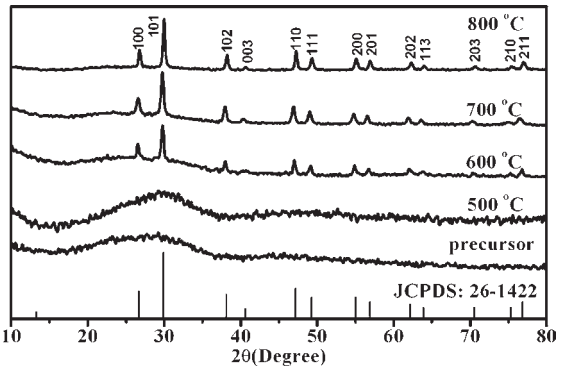

Figure 1. XRD patterns for the precursor and $Gd_2O_2S:Eu^{3+}$ submicrospheres annealed at different temperatures as well as the data of Gd_2O_2S, JCPDS card no. 26−1422, for comparison.

2.2. Characterization. Powder X-ray diffraction (XRD) measurements were performed on a Bruker D8 focus X-ray powder diffractometer with Cu Kα radiation (λ = 0.15405 nm). Elemental analysis of C, H, and N were carried out on VarioEL (Elementar Analysensysteme GmbH). Fourier transform infrared spectroscopy (FT-IR) spectra were measured with the Perking-Elmer 580B infrared spectrophotometer using the KBr pellet technique. The size and morphology of the samples were inspected using a field emission scanning electron microscope equipped with an energy-dispersive spectrometer (EDS) (FE-SEM, S-4800, Hitachi, Japan). The transmission electron microscopy (TEM) and selected area electron diffraction (SAED) patterns were obtained by a JEOL-2010 transmission electron microscope at the accelerating voltage of 200 kV. Photoluminescence (PL) excitation and emission spectra were recorded with a Hitachi F-4500 spectrophotometer equipped with a 150 W xenon lamp as the excitation source at room temperature. The luminescence decay curves were obtained from a Lecroy Wave Runner 6100 Digital Oscilloscope (1 GHz) using a tunable laser (pulse width = 4 ns, gate = 50 ns) as the excitation source (Continuum Sunlite OPO). All the measurements were performed at room temperature.

3. Results and Discussion

3.1. Structures. Figure 1 shows the XRD patterns of the as-prepared precursor sample and those annealed from 500 to 800 °C, as well as the data of Gd_2O_2S (JCPDS No. 26−1422), respectively. There are two broad peaks near 2θ = 28.55° and 47.26° in the curve of the precursor, indicating that the precursor is composed of amorphous gadolinium compound. According to the results of EDS (Supporting Information, Figure S1) and element analysis measurement, the precursor is composed of Gd, Eu, C (5.373 wt %), O, N (0.842 wt %), H (1.5105 wt %), and S elements. The FT-IR spectra of the precursor synthesized with and without PVP are shown in Figure 2. Compared with curve (b), curve (a) has two additional absorption peaks located at 1296 and 1658 cm^{-1}, which can be attributed to the stretching mode of the tertiary amine group and C=O, respectively.[20] This result may be indicative of the existence of PVP in the precursors. The band at 1520 cm^{-1} is attributed to the C−N stretching vibration which appears at 1474 cm^{-1} in pure thiourea. The blue shift of the C−N stretching vibration implies that the sulfur atom of the thiourea was

(12) Thirumalai, J.; Jagannathan, R.; Trivedi, D. C. *J. Lumin.* **2007**, *126*, 353.
(13) Kawahara, Y.; Petrykin, V.; Ichihara, T.; Kijima, N.; Kakihana, M. *Chem. Mater.* **2006**, *18*, 6303.
(14) Dhanaraj, J.; Geethalakshmi, M.; Jagannathan, R.; Kutty, T. R. N. *Chem. Phys. Lett.* **2004**, *387*, 23.
(15) Liu, Z.; Sun, X.; Xu, S.; Lian, J.; Li, X.; Xiu, Z.; Li, Q.; Huo, D.; Li, J. G. *J. Phys. Chem. C.* **2008**, *112*, 2353.
(16) Huang, Y. Z.; Chen, L.; Wu, L. M. *Cryst. Growth Des.* **2008**, *8*, 739.
(17) (a) Zhao, F.; Yuan, M.; Zhang, W.; Gao, S. *J. Am. Chem. Soc.* **2006**, *128*, 11758. (b) Hang, T.; Liu, Q.; Mao, D.; Chang, C. *Mater. Chem. Phys.* **2008**, *107*, 142. (c) Thirumalai, J.; Chandramohan, R.; Divakar, R.; Mohandas, E.; Sekar, M.; Parameswaran, P. *Nanotechnology* **2008**, *19*, 395703.
(18) Martinez-Rubio, M. I.; Ireland, T. G.; Fern, G. R.; Silver, J.; Snowden, M. J. *Langmuir* **2001**, *17*, 7145.
(19) (a) Zhang, Q.; Yao, W.-T.; Chen, X.; Zhu, L.; Fu, Y.; Zhang, G.; Sheng, L.; Yu, S.-H. *Cryst. Growth Des.* **2007**, *7*, 1423. (b) Deng, H.; Li, X. L.; Peng, Q.; Wang, X.; Chen, J.; Li, Y. D. *Angew. Chem., Int. Ed.* **2005**, *44*, 2782.
(20) Patel, J. D.; Chaudhuri, T. K. *Mater. Res. Bull.* **2009**, *44*, 1647.

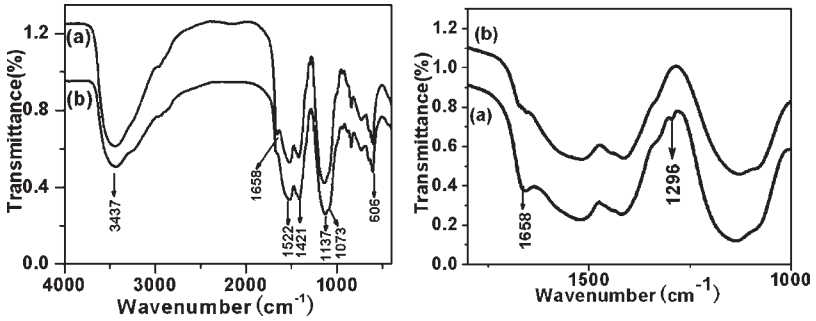

Figure 2. FT-IR spectra of the precursors synthesized at 200 °C for 24 h with (a) and without (b) PVP.

coordinated to the metal ion in the precursor.[21] The C=S stretching vibration at 1084 cm^{-1} in pure thiourea appears as a doublet in the precursor at 1137 and 1073 cm^{-1}, further confirming the existence of Gd−S bond.[21] The absorption peak at 606 cm^{-1} may signify the presence of δ(Gd−S) mode.[22] But the precise structure of the precursor cannot be obtained and needs to be probed further.

After being annealed at 500 °C, the sample remains amorphous. When the temperature is higher than 600 °C, well-defined diffraction peaks appear; all of them can be indexed to the hexagonal phase of Gd_2O_2S according to the data of JCPDS card no. 26−1422, suggesting that the precursor sample has begun to crystallize into Gd_2O_2S at this heating temperature. Further increasing the annealing temperature from 600 to 800 °C, the peaks become even sharper and stronger, which is due to the increase of crystallinity.

In general, the nanocrystallite size can be estimated from the Scherrer equation, $D = 0.941\lambda/\beta \cos \theta$, where D is the average grain size, the factor 0.941 is characteristic of spherical objects, λ is the X-ray wavelength (0.15405 nm), and β and θ are the full width at half-maximum and the diffraction angle (in radians) of an observed peak, respectively.[23] The strongest peaks (101) at 2θ = 30.153, 29.971, 29.770° are used to calculate the average crystallite size (D) of the Gd_2O_2S:0.05Eu^{3+} particles from 600 to 800 °C. The estimated average crystallite sizes are about 25, 28, and 32 nm. The crystallite sizes become bigger with the increase of the postcalcining temperature.

3.2. Morphology. Scanning electron microscopy (SEM) and TEM were used to characterize the morphology and crystal structure of the products. Figure 3A and B shows typical SEM images of solvothermal precursors at 200 °C, revealing that the precursors consist of separated spheres with diameter of 210−300 nm. After being annealed at 600 °C, the obtained Gd_2O_2S:Eu^{3+} products inherited the spherical shape from the precursor. But their average diameter is reduced to 140−220 nm (Figure 3C) because of the decomposition of the precursor. If the postcalcining temperature is higher (800 °C), the spherical morphologies still are retained in good condition, as shown in Figure 3D. Their sizes change little compared with that of the product in Figure 3C. The decrease in size from hydrothermal precursor to relevant oxide through thermic decomposition is common for lanthanum compounds and others.[24] In addition, high magnification SEM images clearly show that the submicrospheres of Gd_2O_2S:Eu^{3+} actually further consist of small grains, and the grain size becomes bigger with the increasing temperature, as shown in Figures 3E and 3F. After being annealed at 800 °C, the grain size is about 25−50 nm. The average nanocrystal size estimated from the Scherrer equation matches well with this result. A typical TEM image and SAED patterns for the Gd_2O_2S:Eu^{3+} sample annealed at 800 °C are shown in Figure 4a, which clearly confirms that the diameter of the Gd_2O_2S:Eu^{3+} submicrospheres is about 140−180 nm and the spheres actually further consist of small grains, consistent with the value shown in the SEM images. The grains aggregate noncompactly and are somewhat hollow as can be seen. This may be attributed to the release of gaseous carbon oxides/sulfides during the calcination process. The SAED image contains partial ring and dot patterns, indicating that the Gd_2O_2S:Eu^{3+} submicrosphere is of polycrystalline nature. The high-resolution transmission electron microscopy (HRTEM) image (Figure 4b) of the nanocrystal composing the Gd_2O_2S:Eu^{3+} submicrosphere clearly shows a lattice fringe with interplanar spacing of 0.331 nm that corresponds to the (100) plane of Gd_2O_2S.

The crystal growth habit is not only determined by the internal structure but also affected by the external conditions. The effect of PVP content, ratio of EG to ethanol, and reaction time on the morphology and size of the precursor are summarized in Table 1. The use of organic surfactants and polymers in the synthesis of nanostructures has been a popular method to achieve morphological control. Recent research has indicated that capping organic molecules in the reaction system could modulate the kinetics of the crystal growth and determine the subsequent morphology of the product.[25] In the present work, PVP plays important roles in the spherical shape formation (Supporting Information, Figure S2). When EG was used as a solvent, a stable Gd-OCH_2CH_2-OH complex was formed like Y-OCH_2CH_2OH and Pb-OCH_2CH_2OH.[24,26] The hydrolysis of the complex produced colloidal sol, where the precursor nanoparticles

(21) (a) Yamaguchi, A.; Penland, R. B.; Mizushima, S.; Lane, T. J.; Curran, C.; Quagliano, J. V. *J. Am. Chem. Soc.* **1958**, *80*, 527. (b) Yang, J.; Zeng, J.; Yu, S.; Yang, L.; Zhang, Y.; Qian, Y. T. *Chem. Mater.* **2000**, *12*, 2924.

(22) (a) Thirumalai, J.; Chandramohan, R.; Valanarasu, S.; Vijayan, T. A.; Somasundaram, R. M.; Mahalingam, T.; Srikumar, S. R. *J. Mater. Sci.* **2009**, *44*, 3889. (b) Vila, L. D.; Stucchi, E. B.; Davolos, M. R. *J. Mater. Chem.* **1997**, *7*, 2113.

(23) Zhang, Y. W.; Jin, S.; Tian, S. J.; Li, G. B.; Jia, T.; Liao, C. S.; Yan, C. H. *Chem. Mater.* **2001**, *13*, 372.

(24) Jia, G.; Yang, M.; Song, Y.; You, H.; Zhang, H. *Cryst. Growth Des.* **2009**, *9*, 301.

(25) Peng, Z.; Jiang, Y.; Song, Y.; Wang, C.; Zhang, H. *Chem. Mater.* **2008**, *20*, 3153.

(26) Geng, J.; Lv, Y. N.; Lu, D. J.; Zhu, J. J. *Nanotechnology* **2006**, *17*, 2614.

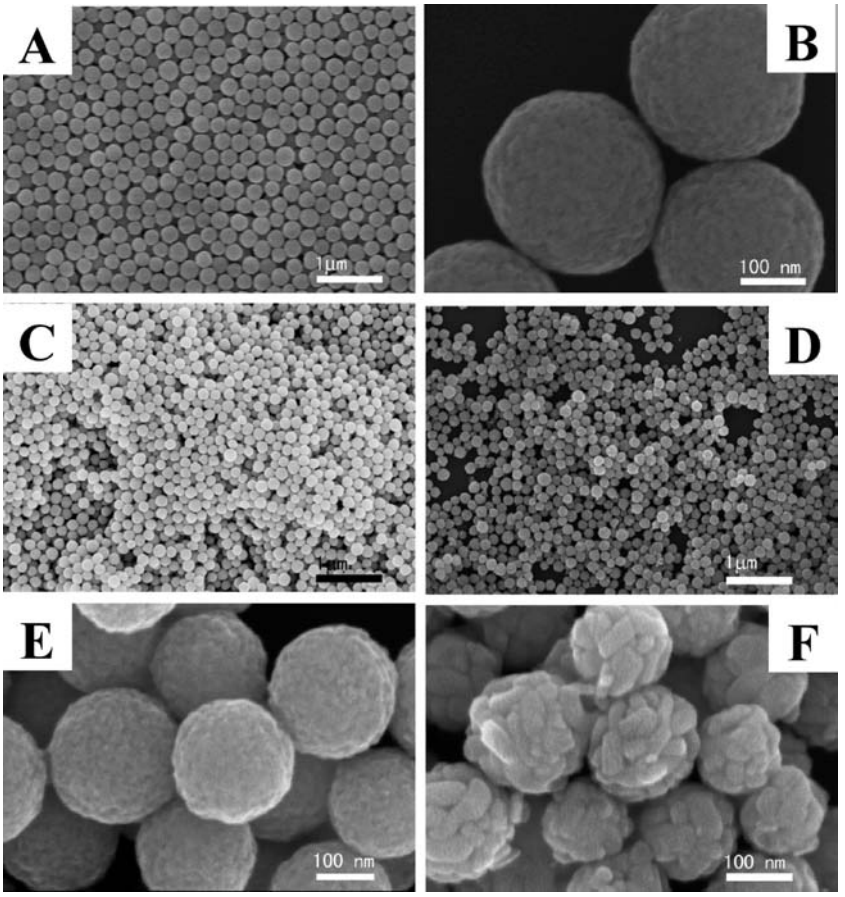

Figure 3. Low- (A) and high (B) magnification SEM images of the solvothermal precursor; $Gd_2O_2S:Eu^{3+}$ spheres after annealing at 600 (C) and 800 °C (D) as well as the high magnification SEM images showing nanoparticles on the surface of the spheres after annealing at 600 (E) and 800 °C(F).

were covered with PVP, and these molecules adsorbed on the surface of the particles formed a protective layer to hold back the growth rate of precursor nanoparticles. When the amount of PVP was higher than 1.0 g, the surfactant concentration was high enough to adsorb on the faces of the particles in all directions to entail isotropic growth, consequently stable spherical submicrospheres were obtained. Although the exact function of PVP on the shape selectivity in our synthetic system was not yet to be fully understood, it was believed that two properties of PVP play a main role in determining the product morphology. One is the strong selective adsorption of PVP on various planes of the nanoparticles. The other is the coordination bonding with the O and N atoms of the pyrrolidone ring.[27] The strong interaction between precursor and PVP led to a relatively large amount of PVP residues in the final product, which was confirmed by the FT-IR curve.

Both the morphology and particle size are also affected by the volume ratio of EG to ethanol in the solvothermal system (Table 1). The more ethanol is added into the system, the bigger the spheres will grow and the smoother the surface will become (Supporting Information, Figure S3). Hence the spherical size can be easily tuned by changing the volume ratio of the solvent. The physical and chemical properties of the solvent can influence the solubility, reactivity, and diffusion behavior of the reagents and intermediate. Since EG was a high viscosity solvent, different amounts of EG led to different diffusion rates of ions in the solution. Consequently, when a higher volume ratio of EG to ethanol was applied as solvent, crystalline growth was suppressed because of the low diffusion rate of ions in the solvent, and led to the formation of smaller spheres. On the other hand, a lower volume ratio of EG to ethanol led to the a high diffusion rate of ions in the solution, and, as a result, bigger spheres were produced.[28]

To further investigate the details of the precursor formation, the growth process of the precursor throughout the solvothermal process was investigated by observing the images of precursor after different solvothermal treatments for (A) 2.5 h, (B) 3 h, (C) 12 h, and (D) 18 h, respectively (Supporting Information, Figure S4). After solvothermal treatment for 2 h, the solution was still transparent. The spherical precursor appeared just after solvothermal treatment of 2.5 h, and the diameter was about 130−200 nm. During the continuous growth of the precursor, the spherical particles had become just a little bigger because of isotropic growth. The growth of the spheres may be inhibited by PVP.

The precursor is converted to $Gd_2O_2S:Eu^{3+}$ during the subsequent calcination process. Nevertheless, the conversion does not lead to the change in the morphology (Supporting Information, Figure S5). Such a transformation is common for lanthanum compounds. The morphologies

(27) (a) Wang, J.; Wang, X.; Peng, Q.; Li, Y. *Inorg. Chem.* **2004**, *43*, 7552. (b) Zhou, F.; Zhao, X.; Xu, H.; Yuan, C. *J. Phys. Chem. C.* **2007**, *111*, 1651.

(28) Xue, F.; Li, H.; Zhu, Y.; Xiong, S.; Zhang, X.; Wang, T.; Liang, X.; Qian, Y. *J. Solid State Chem.* **2009**, *182*, 1396.

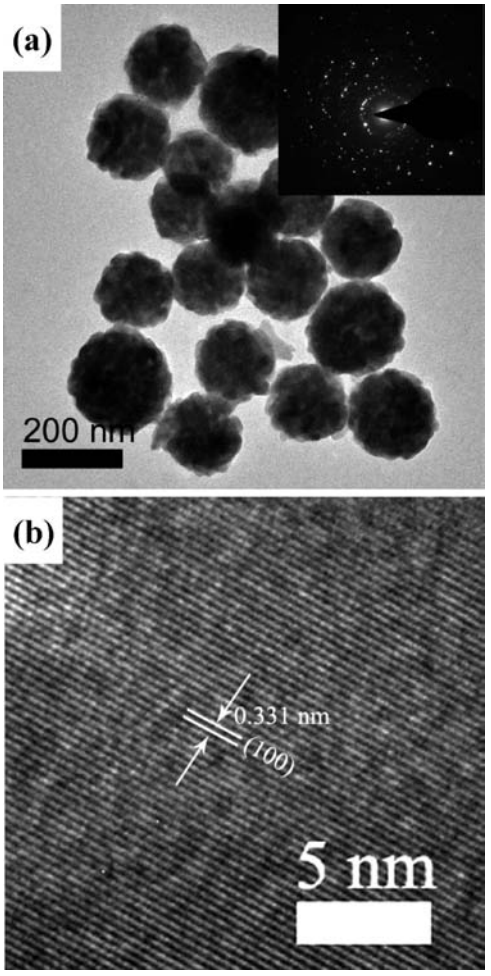

Figure 4. TEM (a) image of the product annealed at 800 °C with its SAED patterns (inset). HRTEM image of the nanocrystal composing the $Gd_2O_2S:Eu^{3+}$ submicrosphere.

Table 1. Effect of PVP Content, Ratio of EG to Ethanol, and Reaction Time on the Morphology and Size

factor		morphology	diameter(μm)
PVP content (g)	0	agglomerate	
	0.5	immature spheres	
	1.0	submicrospheres	0.205−0.285
	2.0	submicrospheres	0.210−0.300
ratio of EG to ethanol	35:0	submicrospheres	0.170−0.240
	30:5	submicrospheres	0.210−0.280
	25:10	submicrospheres	0.210−0.300
	10:25	submicrospheres	0.550−0.790
	0:35	microspheres	0.900−1.25
reaction time (h)	2.5	submicrospheres	0.130−0.200
	3	submicrospheres	0.194−0.293
	12	submicrospheres	0.235−0.304
	18	submicrospheres	0.240−0.310

are maintained perhaps because of the higher activation energies needed for the collapse of these structures.[29]

3.3. Luminescence Properties. Figure 5A shows the excitation and emission spectra of the $Gd_2O_2S:Eu^{3+}$ submicrospheres synthesized at 800 °C. The excitation spectrum is composed of a broadband from 200 to 400 nm and some weakly sharp peaks from 400 to 500 nm. The broad excitation bands ranging from 200 to 400 nm can

(29) Zhang, F.; Braun, G. B.; Shi, Y.; Zhang, Y.; Sun, X.; Reich, N. O.; Zhao, D.; Stucky, G. *J. Am. Chem. Soc.* **2010**, *132*, 2850.

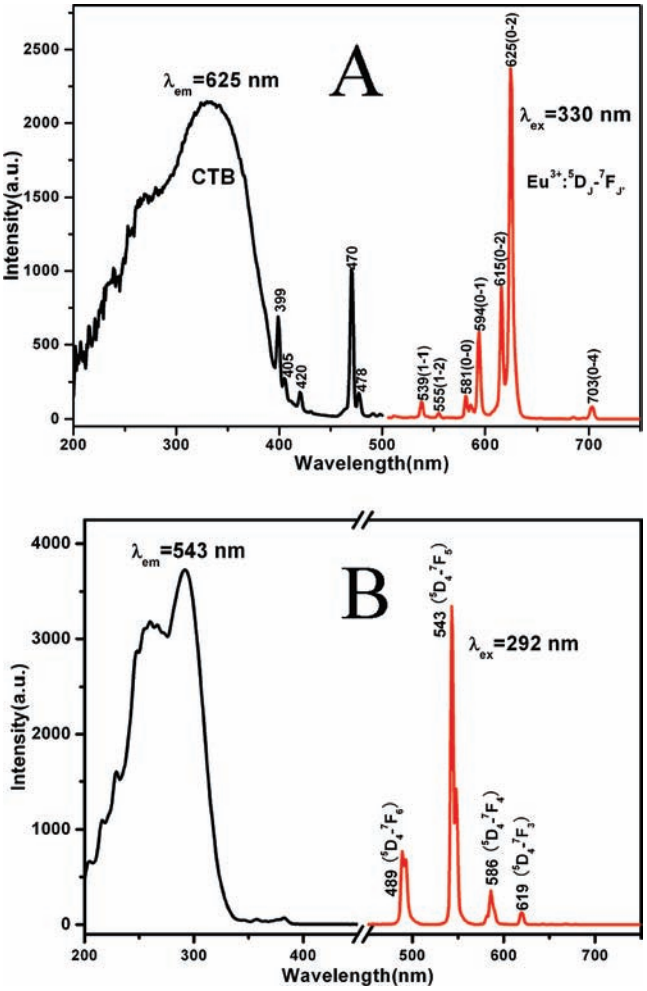

Figure 5. Excitation and emission spectra of $Gd_2O_2S:Eu^{3+}$ (A) and $Gd_2O_2S:Tb^{3+}$ (B).

be ascribed to the charge transfer band (CTB) between the anions and the Eu^{3+} ions. The one around 260 nm is attributed to $O^{2-}\rightarrow Eu^{3+}$ transition and the other one around 330 nm is attributed to the $S^{2-}\rightarrow Eu^{3+}$ transition. In the longer wavelength region, the f-f transition lines of the Eu^{3+} ions can be observed with very weak intensity compared with that of the CTB. Upon excitation at 330 nm, the emission spectrum consists of the $^5D_{0,1}\rightarrow{}^7F_J$ (J = 0, 1, 2, 4) transition lines of the Eu^{3+} ions. The strongest red emission which splits into two peaks at 625 and 615 nm arises from the forced electric-dipole $^5D_0\rightarrow{}^7F_2$ transitions of the Eu^{3+} ions. All the other emission peaks are assigned to the $^5D_1\rightarrow{}^7F_1$ (539 nm), $^5D_1\rightarrow{}^7F_2$ (555 nm), $^5D_0\rightarrow{}^7F_0$ (581 nm), $^5D_0\rightarrow{}^7F_1$ (586, 594 nm), and $^5D_0\rightarrow{}^7F_4$ (703 nm) transitions of the Eu^{3+} ions, respectively.

Figure 5B shows the excitation and emission spectra of the $Gd_2O_2S:Tb^{3+}$ submicrospheres. The excitation spectrum is composed of a broad band and some weak lines in the longer wavelength. The broad bands at about 260 and 292 nm can be ascribed to the spin allowed and spin-forbidden 4f→5d transition of the Tb^{3+} ions, respectively. The remaining peaks with weaker intensity are assigned to the transitions from the $^7F_6$ ground state to the different excited states of the Tb^{3+} ions, that is, $^5G_2$ (346 nm), $^5D_2$ (358 nm), $^5G_6$ (371 nm), and $^5D_3$ (382 nm), respectively. Upon the excitation at 292 nm, the obtained emission

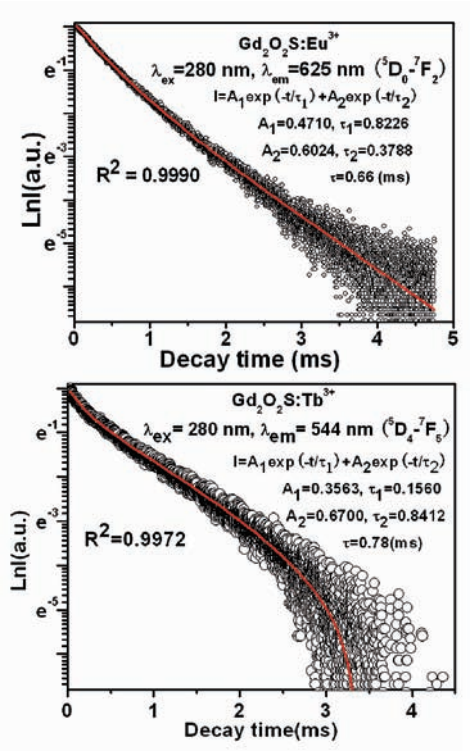

Figure 6. Decay curves of Eu^{3+} and Tb^{3+} luminescence in crystalline Gd_2O_2S submicrospheres. Round circles: experimental data; Red solid line: fitting results.

spectrum exhibits four obvious lines centered at 489, 543, 586, and 619 nm, that can be attributed to the transitions from the $^5D_4$ excited-state to the ^7F_J ($J = 6, 5, 4, 3$) ground states of the Tb^{3+} ion, respectively. The $^5D_4 \rightarrow {}^7F_5$ transition at 543 nm is the most prominent group. The quantum yields of Gd_2O_2S:Eu^{3+} and Gd_2O_2S:Tb^{3+} have been measured, and the values are 7.7% and 14.6%, respectively.

The PL decay curves for the luminescence of the Eu^{3+} and Tb^{3+} ions in Gd_2O_2S submicrospheres are shown in Figure 6. Both the curves can be well fitted by a biexponential function such as $I = A_1 \exp(-t/\tau_1) + A_2 \exp(-t/\tau_2)$, and the average lifetimes for the Eu^{3+} and Tb^{3+} ions are determined to be 0.66 and 0.78 ms, respectively, which are shorter than that of the bulk.[14,15] In some rare-earth doped oxide nanocrystals, it was observed that the luminescent lifetime decreased with the decrease of nanocrystal size, while in the other nanocrystals, the lifetime increased with the decrease of nanocrystal size. The former fact is generally attributed to the increase of non-radiative transition rate caused by surface defects in nanocrystals, whereas the latter fact is usually attributed to decreased radiative transition rate induced by the variation of effective refractive index. The radiative transition rate can be derived as follows:

$$\tau_R \approx \frac{1}{f(\mathrm{ED})} \frac{\lambda_0^2}{\left[\frac{1}{3}(n^2+2)\right]^2 n}$$

Where f(ED) is the oscillator strength for the electronic dipole transition, λ_0 is the wavelength in vacuum, and n is the refractive index of the material. Meltzer et al. observed that the radiative lifetime of the nanocrystals depended not only on the refractive index itself but also on the surrounding medium and deduced that n in the above equation should be substituted by the effective index $n_{eff} = xn + (1 - x)n_{med}$, where x is the filling factor showing what fraction of the space is occupied by the nanoparticles and n_{med} is the refractive index of the surrounding media.[9,30] Compared with the lifetime reported by Dhanaraj et al.,[14] the shortening of the lifetime may be mainly due to the increased non-radiative rate. The increase in non-radiative rates may be rationalized in terms of pronounced phonon-losses, non-radiative energy losses through channels related to defect-centers arising from surface states of the nanocrystals.

4. Conclusion

In summary, well dispersed and homogeneous Gd_2O_2S:Ln^{3+} (Ln = Eu, Tb) submicrospheres have been successfully achieved by a facile solvothermal method combining with a postcalcining process. The PVP plays important roles for the formation of the spherical morphology, and the formation mechanism has been proposed to be an isotropic growth process. The spherical size can be modulated from 170 nm to 1.25 μm by changing the volume ratio of EG to ethanol in the solvent. Under the UV excitation, the Gd_2O_2S:Ln^{3+} (Ln = Eu, Tb) submicrospheres exhibit red and green emissions, respectively. The lifetimes for Gd_2O_2S:Eu^{3+} and Gd_2O_2S:Tb^{3+} are 0.66 and 0.78 ms, respectively. It is expected that our synthetic approach may open a new way for monodisperse spheres that exhibit promising physicochemical properties.

Acknowledgment. This work is financially supported by the National Natural Science Foundation of China (Grant 20771098) and the NSFC Fund for Creative Research Groups (Grant 20921002), and the National Basic Research Program of China (973 Program, Grants 2007CB935502 and 2006CB601103).

Supporting Information Available: The EDS spectrum of the precursor (Figure S1); SEM images for the solvothermal precursors prepared with different amount of PVP (Figure S2); SEM images for the solvothermal precursors prepared with different ratio of EG to ethanol (Figure S3); SEM images of the products obtained at different reaction times (Figure S4); SEM images for the Gd_2O_2S:Eu^{3+} prepared with different ratio of EG to ethanol and annealed at 800 °C under N_2/S atmosphere (Figure S5). This material is available free of charge via the Internet at http://pubs.acs.org.

(30) (a) Meltzer, R.; Feofilov, S.; Tissue, B. *Phys. Rev. B* **1999**, *60*, 14012. (b) Peng, H.; Song, H.; Chen, B.; Wang, J.; Lu, S.; Kong, X.; Zhang, J. *J. Chem. Phys.* **2003**, *118*, 3277.